

Exact simulation of pigment-protein complexes unveils vibronic renormalization of electronic parameters in ultrafast spectroscopy

F. Caycedo-Soler¹, A. Mattioni ¹, J. Lim¹, T. Renger ², S. F. Huelga ^{1✉} & M. B. Plenio ^{1✉}

The primary steps of photosynthesis rely on the generation, transport, and trapping of excitons in pigment-protein complexes (PPCs). Generically, PPCs possess highly structured vibrational spectra, combining many discrete intra-pigment modes and a quasi-continuous of protein modes, with vibrational and electronic couplings of comparable strength. The intricacy of the resulting vibronic dynamics poses significant challenges in establishing a quantitative connection between spectroscopic data and underlying microscopic models. Here we show how to address this challenge using numerically exact simulation methods by considering two model systems, namely the water-soluble chlorophyll-binding protein of cauliflower and the special pair of bacterial reaction centers. We demonstrate that the inclusion of the full multi-mode vibronic dynamics in numerical calculations of linear spectra leads to systematic and quantitatively significant corrections to electronic parameter estimation. These multi-mode vibronic effects are shown to be relevant in the longstanding discussion regarding the origin of long-lived oscillations in multidimensional nonlinear spectra.

¹Institute of Theoretical Physics and IQST, Ulm University, Albert-Einstein-Allee 11, 89081 Ulm, Germany. ²Institute of Theoretical Physics, Department of Theoretical Biophysics, Johannes Kepler University Linz, Altenberger Str. 69, 4040 Linz, Austria. ✉email: susana.huelga@uni-ulm.de; martin.plenio@uni-ulm.de

Light-harvesting (LH) antennas and photo-chemical reaction centers (RC) provide the elementary building blocks of the photosynthetic apparatus of plants, algae, and bacteria¹. Primarily these molecular aggregates consist of absorbing molecules (pigments) complexed with specific proteins to form a PPC. Despite its fundamental importance to biology, the dynamical characterization of these complexes to a degree that can reproduce all reported spectroscopic data in a single microscopic model remains an outstanding challenge.

Reduced models of excitonic dynamics subject to purely thermal fluctuations can achieve reasonable agreement with linear optical spectra^{2–9}. The quantitative explanation of all relevant aspects of multi-dimensional nonlinear spectroscopy though requires a more detailed model of the system-environment interaction that takes into account the full complexity of the environmental structure¹⁰. Indeed, spectroscopic studies of PPCs at low temperatures^{11–14} reveal the presence of vibrational environments that consist of a broad spectrum of low-frequency protein modes with room temperature energy scales, and several tens of discrete high-frequency modes that originate mainly from intra-pigment dynamics^{11,12,15}. Nonlinear optical experiments on monomer pigments in solution at both 77 K^{16,17} and room temperature^{18,19}, as well as first-principles calculations^{20,21} further corroborate the underdamped nature of intra-pigment vibrational modes with picosecond lifetimes.

Recently, a range of vibronic models in which pigments are subject to the combined influence of a broad unstructured bosonic environment and a small number of vibrational modes with frequencies in the vicinity of excitonic transitions have been formulated^{22–31}. In this picture, vibrational lifetime borrowing can lead to long-lasting oscillatory dynamics of coherences between excitonic states, and observations of long-lasting oscillatory features in multi-dimensional spectroscopy^{32–37} have been attributed to this effect^{38–43}. Notwithstanding, the identification of a universally accepted origin of these long-lived oscillations remains a subject of active discussion^{34,44–47}.

An important obstacle that prevents the conclusive resolution of this debate is the fact that the interpretation of spectroscopic data and their underpinning dynamical features can be influenced significantly by the specific choice of electronic and vibrational parameters that enter the PPC models. We will demonstrate that by accounting for the full environmental spectral density, involving more than 50 intra-pigment modes per site in addition to a broad background, the presence of high-frequency long-lived vibrational modes can lead to quantitatively significant modification of the calculated linear spectra of PPCs and consequently the estimated values of electronic parameters to recover a best fit with actual measurements. These corrections do not appear when considering only selected resonant modes and go well beyond predictions obtained by using conventional line shape theory^{48–51}.

To present our results, we provide an analytical theory of renormalization effects due to multi-mode vibronic mixing in model excitonic systems of two prototypical PPCs, namely the water-soluble chlorophyll-binding protein (WSCP) of cauliflower and the special pair (SP) of bacterial reaction centers, depicted in Fig. 1. By considering realistic environmental spectral densities, we corroborate our predictions using two independent numerically exact methods (the temperature-dependent time evolving density matrix using orthogonal polynomials algorithm, T-TEDOPA^{22,52–54}, and the hierarchical equations of motion, HEOM⁵⁵). We show that the hybridization of electronic and vibrational degrees of freedom requires a significant renormalization of electronic couplings. Importantly, this renormalization of electronic parameters, in turn, is shown to have a significant impact on the dynamics of excitonic coherences, notably the lifetimes of their oscillatory dynamics.

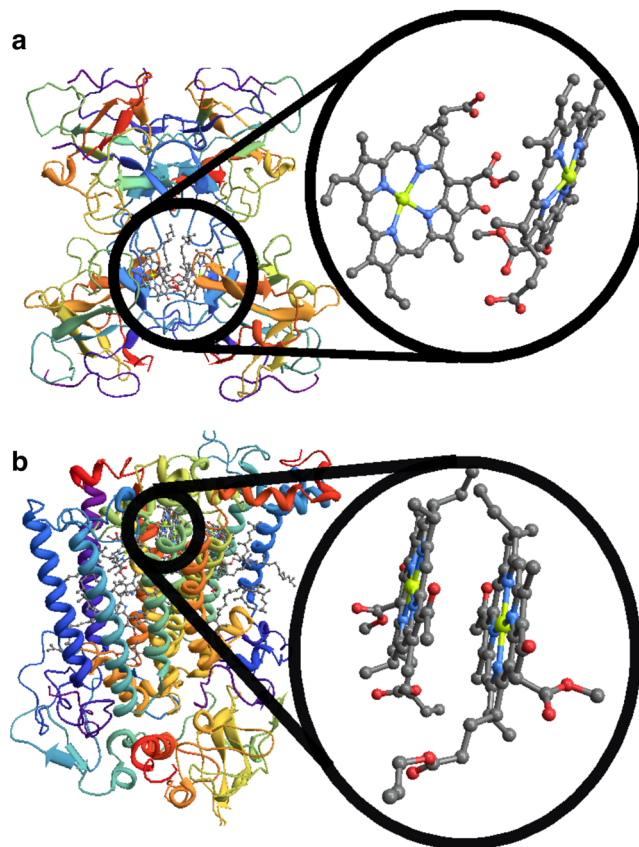


Fig. 1 Photosynthetic pigment-protein complexes. **a** Molecular structure of water-soluble chlorophyll-binding protein from cauliflower, a natural dimeric PPC, with Chlb homodimer shown in detail. **b** Molecular structure of bacterial reaction center from purple bacterium *Rb. Sphaeroides* with a (hetero)-dimeric unit of special pair highlighted. Site energies and couplings for the relevant pigments are obtained from models that combine the crystal structure together with a comparison of calculated and measured spectra⁷⁰.

Results

Electronic and vibronic couplings of PPCs. Absorption spectra of PPCs are determined by the electronic energy-level structure of pigments, their mutual electronic interactions and the coupling of the resulting excitons to vibrational degrees of freedom of the pigment's environment. In the following, we will restrict our analysis to the Q_y transition between electronic ground and first excited states of the pigments, which suffices for the evaluation of the low-energy part of absorption spectra and is relevant for photosynthetic energy transfer¹. For the dimeric WSCP and SP, the electronic Hamiltonian is then described by (see Supplementary Note 1)

$$H_e = \sum_{i=1}^2 \varepsilon_i |\varepsilon_i\rangle \langle \varepsilon_i| + V(|\varepsilon_1\rangle \langle \varepsilon_2| + |\varepsilon_2\rangle \langle \varepsilon_1|). \quad (1)$$

Here $|\varepsilon_i\rangle$ denotes the singly excited state of site i with on-site energy ε_i that is in the visible (WSCP) or in the near infrared spectrum (SP). The on-site energies depend on their local environment and therefore suffer from static disorder inducing ensemble dephasing that will be included in our numerical treatment. The electronic coupling V leads to delocalized electronic eigenstates (excitons), $H_e |E_{\pm}\rangle = E_{\pm} |E_{\pm}\rangle$, and an excitonic splitting $\Delta = E_+ - E_- = \sqrt{4V^2 + (\varepsilon_1 - \varepsilon_2)^2}$. In WSCP, the mean site energies are identical, $\langle \varepsilon_1 \rangle = \langle \varepsilon_2 \rangle$, due to the symmetry

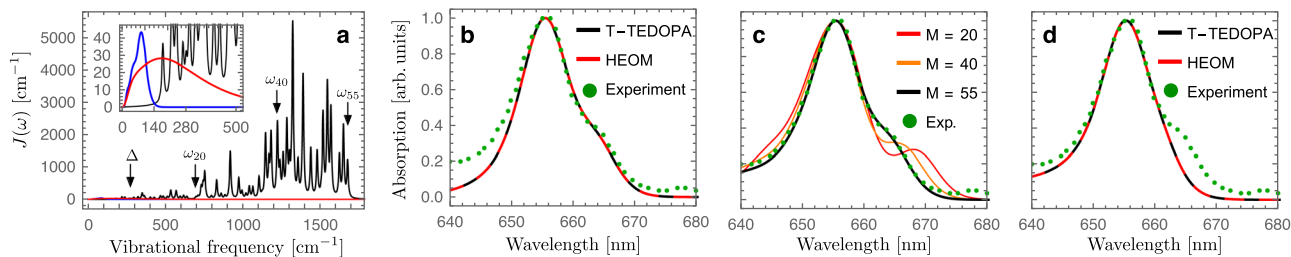


Fig. 2 Absorption spectra of WSCP. **a** Experimentally estimated spectral density of WSCP, consisting of 55 intra-pigment modes $J_h(\omega)$ ¹³ and low-frequency protein modes $J_l^{WSCP}(\omega)$ ⁵⁸, shown in black and blue, respectively. Experimentally estimated spectral density $J_l^{B777}(\omega)$ of B777 complexes is shown in red⁶⁰. The position of the excitonic splitting $\Delta = 280 \text{ cm}^{-1}$ obtained for an electronic coupling $V = 140 \text{ cm}^{-1}$ is indicated by a black arrow. The 20th, 40th and 55th lowest vibrational frequencies of the intra-pigment modes are marked by black arrows with ω_{20} , ω_{40} , and ω_{55} , respectively. **b** Experimental absorption spectrum of WSCP at 77 K, shown in green dots, and numerical results obtained by T-TEDOPA and HEOM, shown in black solid and red dashed lines, respectively, for $V = 69 \text{ cm}^{-1}$ and $J_l^{B777}(\omega)$ ⁶⁰. **c** For $V = 140 \text{ cm}^{-1}$ and $J_l^{WSCP}(\omega) + J_h(\omega)$, T-TEDOPA and HEOM results can reproduce the experimental absorption spectrum, as shown in black. Numerically exact absorption spectra for the $M \in \{20, 40, 55\}$ lowest frequency intra-pigment modes are displayed where $M = 55$ represents the full experimentally estimated spectral density. **d** For $V = 69 \text{ cm}^{-1}$ and $J_l^{WSCP}(\omega) + J_h(\omega)$, T-TEDOPA and HEOM results cannot reproduce the experimental absorption spectra. See Supplementary Note 5 for details of the other molecular parameters used in these simulations. We note that the maximum amplitudes of simulated absorption spectra at 656 nm are normalized to unity for a comparison with experimental absorption line shape.

of molecular structure, while in SP, the mean site energies are different as pigments are surrounded by nonidentical local protein environments. Another difference concerns the electronic coupling strength, which is stronger in SP due to electron exchange giving rise to short-range Dexter type contributions^{56,57}.

The exciton dynamics of PPCs is driven by vibrational modes that induce fluctuations in the transition energies ϵ_i of pigments. The full electronic-vibrational interaction, induced by N vibrational modes per site, is described by the Hamiltonian $H = H_e + H_v + H_{e-v}$ where

$$H_v = \sum_{i=1}^2 \sum_{k=1}^N \omega_k b_{i,k}^\dagger b_{i,k}, \quad (2)$$

$$H_{e-v} = \sum_{i=1}^2 |\epsilon_i\rangle \langle \epsilon_i| \sum_{k=1}^N \omega_k \sqrt{s_k} (b_{i,k} + b_{i,k}^\dagger). \quad (3)$$

Here the annihilation (creation) operator $b_{i,k}$ ($b_{i,k}^\dagger$) describes a local vibrational mode of frequency ω_k coupled to site i with a strength quantified by the Huang-Rhys (HR) factor s_k . For an environment initially in a thermal state, the ensuing dynamics is fully determined by the environmental spectral density $J(\omega) = \sum_k \omega_k^2 s_k \delta(\omega - \omega_k)$ whose structure needs to be determined experimentally or theoretically.

Structure of the environmental spectral density. Generally, in PPCs the spectral density $J(\omega)$ consists of a broad background and multiple sharp peaks distributed across a broad range of frequencies. These can be determined by fluorescence line-narrowing (FLN) and hole burning experiments which reveal that the environmental spectral densities of WSCP and SP consist of low-frequency broad features originating from protein motions, and 55 intra-pigment modes resulting in multiple narrow peaks in the high-frequency part of the spectrum. The contribution of the protein modes of WSCP may be described by log-normal distribution functions of the form $J_l^{WSCP}(\omega) = \sum_m (\omega c_m / \sigma_m) \exp(-[\ln(\omega / \Omega_m)]^2 / 2\sigma_m^2)$, which provides a satisfactory description of the low-energy part of experimentally measured FLN spectra of WSCP⁵⁸. Alternatively, the protein motions of WSCP have been modeled by the following functional form: $J_l^{B777}(\omega) = \frac{S}{s_1 + s_2} \sum_{i=1}^2 \frac{s_i}{7! 2\omega_i^7} \omega^5 e^{-(\omega/\omega_i)^{1/2}}$ that has been extracted from FLN spectra of B777 photo-synthetic complexes⁵⁹ and considered in the simulations of WSCP⁶⁰. Every underdamped intra-pigment mode contributes a

Lorentzian of width $\gamma_k \sim 1 \text{ ps}^{-1}$, resulting in $J(\omega) = J_l(\omega) + J_h(\omega)$ where

$$J_h(\omega) = \sum_{k=1}^{55} \frac{4\omega_k s_k \gamma_k (\omega_k^2 + \gamma_k^2) \omega}{\pi((\omega + \omega_k)^2 + \gamma_k^2)((\omega - \omega_k)^2 + \gamma_k^2)}, \quad (4)$$

and the reorganization energy of the high-frequency modes is given by $\lambda_h = \int_0^\infty d\omega J_h(\omega) / \omega = \sum_{k=1}^{55} \omega_k s_k$. The reorganization energy of the 55 intra-pigment modes of WSCP¹³ (SP¹⁵) is 660 cm^{-1} (379 cm^{-1}), which is several times larger than that of quasi-continuous protein spectrum^{58,61} and quasi-resonant intra-pigment modes with $\omega_k \approx \Delta$ (see Supplementary Note 5). The presence of underdamped vibrational modes can lead to long-lived correlations between electronic and vibrational degrees of freedom that make the rigorous numerical treatment of the ensuing vibronic dynamics very costly. In non-perturbative HEOM simulations, where experimentally or theoretically estimated spectral densities are fitted by the sum of Drude-Lorentz peaks^{21,62}, the simulation cost of a dimeric system exceeds several hundreds of terabytes when 55 intra-pigment modes are considered per site (see Supplementary Note 4) and, therefore, is infeasible with current computer architectures. In this work, we employ T-TEDOPA method where an experimentally estimated vibrational spectral density is mapped to a one-dimensional chain of quantum harmonic oscillators whose complexity is unaffected by the number of long-lived intra-pigment modes in the spectral density. We also employ optimized HEOM method where simulation parameters are determined by fitting the bath correlation function of highly structured environments for a finite time window corresponding to the line width of experimentally measured absorption spectra. These two methods enable one to consider the full environmental structures of WSCP and SP with a moderate simulation cost of the order of a few gigabytes or less (see Supplementary Notes 3 and 4). In addition, numerically exact results obtained by these two independent methods coincide, demonstrating the high accuracy and reliability of our simulated data (see Supplementary Note 6).

WSCP homodimer. The electronic parameters of PPCs have been estimated based on a comparison of experimentally measured spectroscopic data with approximate theoretical results where environmental structures are coarse-grained or vibronic couplings are treated perturbatively. Based on a coarse-grained spectral density $J_l^{B777}(\omega)$, shown in red in Fig. 2a, a best fit to the experimental absorption spectra of WSCP homodimers implies

an electronic coupling strength estimate of $V \approx 70 \text{ cm}^{-1}$ ⁶¹, as shown in red in Fig. 2b. Such an electronic coupling results in an excitonic splitting $\Delta \approx 2V \approx 140 \text{ cm}^{-1}$ which is consistent with the experimentally observed energy-gap between two absorption peaks at 656 and 662 nm, respectively. Since all the high-frequency intra-pigment modes are neglected in the coarse-grained spectral density and the energy-gap between absorption peaks is smaller than the vibrational frequencies of the intra-pigment modes ($\Delta < \omega_k$), the estimated value could be interpreted as the effective coupling V_{00} between $|\varepsilon_1, 0\rangle$ and $|\varepsilon_2, 0\rangle$ where $|0\rangle$ denotes the common vibrational ground state of the intra-pigment modes in the electronic excited state manifold. As shown in Fig. 3a, the transition dipole strength between $|g, 0\rangle$ and $|\varepsilon_i, 0\rangle$ (0-0 transition) of a monomer is reduced by a factor of $\exp(-\sum_k s_k/2)$, as the total transition dipole strength of the monomer is redistributed to 0-1 transitions between $|g, 0\rangle$ and $|\varepsilon_i, 1_k\rangle$ where only the k -th mode is singly excited (see Supplementary Note 10). As a result, the effective coupling between 0-0 transitions, shown in Fig. 3b, is reduced to $V_{00} = V \exp(-\sum_k s_k)$ depending on the HR factors s_k of the intra-pigment modes. This implies that $V_{00} \approx 70 \text{ cm}^{-1}$ corresponds to a bare electronic coupling $V = V_{00} \exp(\sum_{k=1}^{55} s_k) \approx 2V_{00} \approx 140 \text{ cm}^{-1}$ under the full environmental spectral density $J^{\text{WSCP}}(\omega) + J_h(\omega)$, including the 55 intra-pigment modes shown in black in Fig. 2a. The renormalised electronic coupling $V \approx 140 \text{ cm}^{-1}$ yields a best fit to experimentally measured absorption spectra, as shown in black in Fig. 2c, when all the $M = 55$ intra-pigment modes are considered in simulations. The energy-gap between absorption peaks is gradually reduced from excitonic splitting $\Delta \approx 2V \approx 280 \text{ cm}^{-1}$ to $\Delta' \approx 2V_{00} \approx 140 \text{ cm}^{-1}$, as the number M of the lowest-frequency intra-pigment modes considered in simulations is increased from 20 via 40 to 55 (see Fig. 2a, c). The electronic coupling $V \approx 70 \text{ cm}^{-1}$ estimated based on the coarse-grained low-frequency spectral density cannot reproduce the experimental results when the full spectral density is considered in simulations, as shown in Fig. 2d. The energy-gap between absorption peaks shown in Fig. 2c, d can be quantitatively well described by the splitting of 0-0 transitions, $2V_{00} = 2V \exp(-\sum_{k=1}^M s_k)$, implying that the effective couplings V_{01} between 0-0 and 0-1 transitions, schematically shown in Fig. 3b, are not strong enough to modify the energy-gap between low-energy absorption peaks of WSCP. However, the weak V_{01} couplings can redistribute the transition dipole strength from 0-0 to 0-1 transitions and significantly modify the high-energy part of absorption spectra, which cannot be described by conventional line shape theory (see Supplementary Note 10).

Multi-mode vibronic mixing in exciton basis. In contrast to WSCP, the bare excitonic splitting of SP is of the order of the typical vibrational frequencies of the intra-pigment modes and the resulting redistribution of oscillator strengths and shifts of optical lines are much more difficult to predict. To qualitatively estimate these effects, we consider second-order perturbation theory starting from the full Hamiltonian $H = H_e + H_v + H_{e-v}$ in the single-exciton manifold. In that case, the vibronic mixing is induced by the relative motion of the intra-pigment modes with identical frequency ω_k , described by $b_k = (b_{1,k} - b_{2,k})/\sqrt{2}$, as the center of mass motion, described by $B_k = (b_{1,k} + b_{2,k})/\sqrt{2}$, merely induces the homogeneous broadening of absorption line shapes without affecting exciton dynamics (see Supplementary Note 1). Hence, we can discard the center-of-mass part of the total Hamiltonian to find $H = H_0 + H_I$ where

$$H_0 = H_e + H_v + \cos(\theta) \sigma_x \sum_{k=1}^{55} \omega_k \sqrt{s_k/2} (b_k + b_k^\dagger), \quad (5)$$

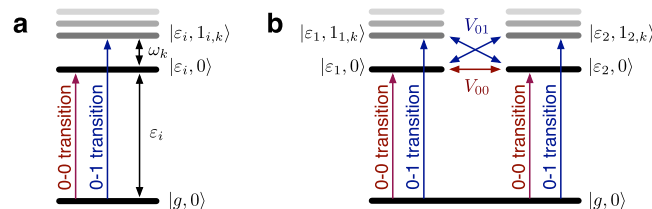


Fig. 3 Vibronic energy-levels in site basis. **a** Energy-level structure of monomer with 0-0 and 0-1 transitions highlighted in red and blue, respectively. **b** Energy-level structure of dimer with V_{00} and V_{01} representing the effective coupling between 0-0 transitions and the interaction between 0-0 and 0-1 transitions, respectively.

with $H_v = \sum_k \omega_k b_k^\dagger b_k$, and

$$H_I = -\sin(\theta) \sigma_x \sum_{k=1}^{55} \omega_k \sqrt{s_k/2} (b_k + b_k^\dagger). \quad (6)$$

Here $\theta = \tan^{-1}[2V/(\varepsilon_1 - \varepsilon_2)]$, while $\sigma_x = |E_+\rangle\langle E_-| + |E_-\rangle\langle E_+|$ and $\sigma_z = |E_+\rangle\langle E_+| - |E_-\rangle\langle E_-|$ are the Pauli matrices in the exciton basis. The Hamiltonian H_0 is diagonalised by the polaron transformation in the exciton basis, $U = |E_+\rangle\langle E_+|D_\theta + |E_-\rangle\langle E_-|D_\theta^\dagger$ with $D_\theta = \exp[\cos(\theta)\sum_k \sqrt{s_k/2}(b_k^\dagger - b_k)]$. For typical HR factors of PPCs, of the order of $s_k \lesssim 0.01$, the vibronic mixing is dominated by contributions from the single vibrational excitation subspace where it leads to eigenstates of H of the form

$$|\psi_\pm\rangle = a_{\pm,0}|E_\pm, 0\rangle + \sum_{k=1}^{55} a_{\mp,1k}|E_\mp, 1_k\rangle, \quad (7)$$

with $|0\rangle$ and $|1_k\rangle$ representing vibrational states where all the intra-pigment modes are in their ground states or only one mode described by b_k is singly excited. In second-order perturbation theory, these vibronic eigenstates $|\psi_\pm\rangle$ have energies

$$E'_\pm = E_\pm \pm \alpha \frac{2V^2}{\Delta^2} \sum_{k=1}^{55} \frac{s_k \omega_k^2}{\Delta \mp \omega_k}, \quad (8)$$

and the purely excitonic splitting $\Delta = E_+ - E_-$ is shifted to a vibronic splitting

$$\Delta' = E'_+ - E'_- = \Delta \left(1 + \alpha \frac{4V^2}{\Delta^2} \sum_{k=1}^{55} \frac{s_k \omega_k^2}{\Delta^2 - \omega_k^2} \right), \quad (9)$$

where $\alpha = \exp(-2\cos^2(\theta)\sum_{k=1}^{55} s_k)$. These energetic corrections are in complete analogy to the well-known light shifts in atomic physics. The sign of these energy shifts is determined by the difference in excitonic splitting and vibrational frequency, $\Delta - \omega_k$. We note that the vibronic energy renormalization can also be described in the regular electronic-vibrational basis without the polaron transformation using second order perturbation theory (see Supplementary Note 2).

For an excitonic splitting that is smaller than the vibrational frequencies, $\Delta \lesssim \omega_k$, the energy-gap Δ' between vibronic eigenstates $|\psi_+\rangle$ and $|\psi_-\rangle$ is reduced compared to the bare excitonic splitting Δ (see Fig. 4a). This is in line with our numerically exact simulations of WSCP where the bare excitonic splitting $\Delta \approx 2V$ is reduced to $\Delta' \approx 2V_{00} \approx V$. It is notable that for PPCs consisting of chlorophylls or bacteriochlorophylls, the HR factors of the intra-pigment modes are of the order of $s_k \approx 0.01$, independent of the vibrational frequencies ω_k . In case the excitonic splitting is significantly smaller than the vibrational frequencies of the intra-pigment modes, the detuning between them is well approximated by $\Delta_k = \omega_k - \Delta \approx \omega_k$, thus exhibiting the same scaling in ω_k as the electronic-vibrational coupling, $g_k = \omega_k \sqrt{s_k}$. This implies that the coupling of higher-frequency modes increases with the detuning

Δ_k so that they cannot simply be ignored on the basis of being off-resonant.

When the excitonic splitting is larger than the vibrational frequencies, $\Delta \gtrsim \omega_k$, the situation is reversed (see Fig. 4b), resulting in an increased vibronic splitting Δ' compared to the bare excitonic splitting Δ . This case cannot be described by the splitting of 0-0 transitions, since the effective coupling $V_{00} = V \exp(-\sum_k s_k)$ is smaller in magnitude than a bare electronic coupling V for arbitrary HR factors defined by $s_k \geq 0$. This implies that the mixing of 0-0 and 0-1 transitions can result in two absorption peaks with an energy gap Δ' being larger than the bare excitonic splitting Δ .

Special pair in bacterial reaction center. The photosynthetic reaction center which drives exciton dissociation into free charges consists of the SP and four additional pigments⁶³. The SP is a strongly coupled dimeric unit with an electronic coupling estimated to be $V = 625 \text{ cm}^{-1}$, a difference in mean site energies of $\langle \epsilon_1 - \epsilon_2 \rangle = 315 \text{ cm}^{-1}$ and consequently a bare excitonic splitting of $\Delta \approx 1290 \text{ cm}^{-1}$. These electronic parameters have been

estimated based on a best fit to absorption, linear dichroism, and hole burning spectra of bacterial reaction centers using conventional line shape theory⁵¹. In what follows, we neglect the order of magnitude weaker electronic coupling of the SP to the four additional pigments and do not aim to reproduce experimentally measured absorption spectra of the whole bacterial reaction centers and re-estimate electronic parameters. Rather we concentrate on the effect of multi-mode vibronic mixing on the SP and its consequences regarding the nature and lifetimes of excitonic coherence and long-lived oscillatory signals in 2D electronic spectra.

While in WSCP the excitonic splitting is far detuned from high-frequency modes, the situation is markedly different for the SP. Here the environmental spectral density contains high-frequency intra-pigment modes both above and below the bare excitonic gap, as shown in black in Fig. 5a. The smaller frequency differences between vibrational modes and excitonic splitting and the varying sign of their detuning makes the effect of multimode mixing harder to predict analytically. Indeed, the perturbation procedure for obtaining Eq. (9) will be inaccurate for a larger number of modes. The vibronic splitting can be estimated beyond the perturbation theory by numerically diagonalising the Hamiltonian $H = H_0 + H_I$ in Eqs. (5), (6), leading to $\Delta' \approx 1744 \text{ cm}^{-1}$ (see Supplementary Note 7). This estimate is in line with numerically exact simulated results where the energy-gap between absorption peaks is approximately 1710 cm^{-1} (see 780 and 900 nm peaks in Fig. 5b, corresponding to $|\psi_+\rangle$ and $|\psi_-\rangle$, respectively) and the oscillatory dynamics of excitonic coherence is dominated by 1755 cm^{-1} frequency component (see Fig. 5c). We note that the difference between excitonic and vibronic splittings is significant, of the order of $\Delta' - \Delta \approx 465 \text{ cm}^{-1}$, and this shift cannot be described by conventional line shape theory where multi-mode vibronic mixing is ignored and as a result the

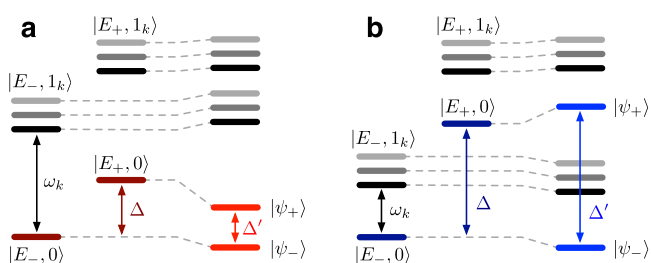


Fig. 4 Vibronic energy-levels in exciton basis. a, b Effect of multi-mode vibronic mixing on vibronic energy-level structure when excitonic splitting Δ is smaller (larger) than vibrational frequencies ω_k of intra-pigment modes, leading to reduction (increment) of the energy gap Δ' between vibronic eigenstates.

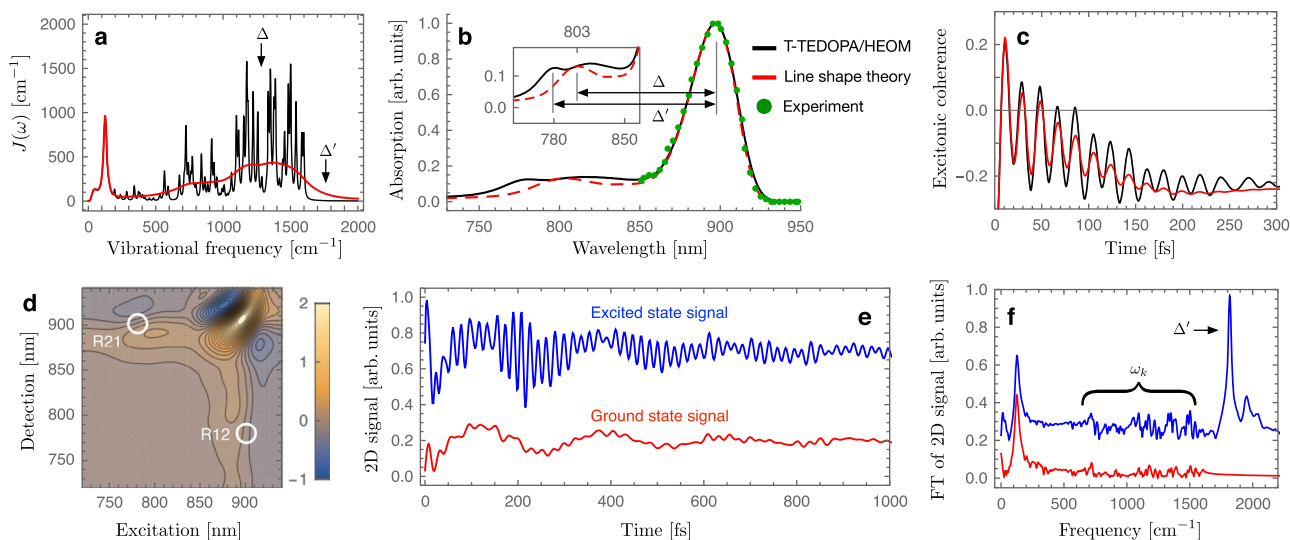


Fig. 5 Absorption and 2D electronic spectra of SP. a Experimentally estimated spectral density of the SP^{15, 61} is shown in black for an intra-pigment mode vibrational damping rate $\gamma_k = (1 \text{ ps})^{-1}$. Coarse-grained version for $\gamma_k = (50 \text{ fs})^{-1}$ is shown in red and the excitonic and vibronic splittings, $\Delta \approx 1290 \text{ cm}^{-1}$ and $\Delta' \approx 1800 \text{ cm}^{-1}$, are highlighted. **b** Experimental absorption spectrum of the bacterial reaction center at 5K, shown in green dots, and numerically exact absorption line shape, obtained by TEDOPA and HEOM, of the SP, shown in black. Approximate absorption spectrum of the SP computed by second-order cumulant expansion is shown in red where the energy-gap between absorption peaks at 803 and 897 nm is approximately $\Delta \approx 1300 \text{ cm}^{-1}$. **c** Excitonic coherence dynamics for the experimentally estimated and coarse-grained environmental structures, shown in black and red, respectively, when only site 1 is initially excited. **d** Rephasing 2D spectra of the SP at waiting time $T = 0$. **e**, **f** 2D signals at a cross-peak R12, marked in (d), and corresponding Fourier transformation where ground and excited state signals are shown in red and blue, respectively. Note that excited state signals are dominated by vibronic coherence $|\psi_+\rangle\langle\psi_-|$, leading to 2D oscillations with frequency $\Delta' \approx 1800 \text{ cm}^{-1}$. The transient of the other cross-peak R21 is provided in Supplementary Note 8 and all molecular parameters used in these simulations are given in Supplementary Note 5.

energy-gap between absorption peaks is reduced to the excitonic splitting (see the inset in Fig. 5b).

Long-lived multi-mode vibronic coherence. The considerable size of the multi-mode mixing effects on excitonic energy gaps suggest a possibly significant influence on coherent excitonic dynamics. The coarse-grained spectral density shown in red in Fig. 5a, which corresponds to a vibrational lifetime of $\gamma_k = (50 \text{ fs})^{-1}$, yields short-lived oscillatory dynamics of excitonic coherence $\rho_{\pm}(t) = \langle E_{\pm} | \hat{\rho}_e(t) | E_{\pm} \rangle$ with $\hat{\rho}_e(t)$ denoting reduced electronic density matrix (see red line in Fig. 5c). Even if a few intra-pigment modes near-resonant with excitonic splitting are selected to be weakly damped, $\gamma_k = (1 \text{ ps})^{-1}$, the vibronic mixing with the large number of remaining strongly-damped modes, $\gamma_k = (50 \text{ fs})^{-1}$, suppresses the lifetime of excitonic coherences, making the resulting dynamics essentially identical to that where all the modes are strongly damped (see Supplementary Note 7 for detailed analysis of multi-mode vibronic mixing). In sharp contrast, when the picosecond lifetime of actual intra-pigment modes is considered, $\gamma_k = (1 \text{ ps})^{-1}$, the excitonic coherence dynamics is dominated by long-lived oscillations with frequency $\Delta' \approx 1755 \text{ cm}^{-1}$, associated with the vibronic coherence between $|\psi_{+}\rangle$ and $|\psi_{-}\rangle$ states (see black line in Fig. 5c).

In 2D electronic spectroscopy, the third-order nonlinear optical response of molecular systems is measured by using a sequence of femtosecond pulses with controlled time delays^{64,65}. As is the case of pump probe experiments⁶⁶, electronically excited state populations and coherences can be created by a pair of pump pulses, and the molecular dynamics in the electronic excited state manifold can be monitored by controlling the time delay T between pump and probe. The additional time delay between two pump pulses enables one to monitor the molecular dynamics as a function of excitation and detection wavelengths for each waiting time T . The optical transitions induced by the pump pulses can also create vibrational coherences in the electronic ground state manifold, making it challenging to extract the information about coherent electronic dynamics from multi-dimensional spectroscopic data⁴⁶.

Our numerically exact simulations of the SP demonstrate that long-lived oscillatory signals in 2D electronic spectra can originate from purely vibrational coherences or from vibronic coherences induced by multi-mode mixing. The latter have been ignored in previous numerical studies which considered only a few intra-pigment modes quasi-resonant with excitonic splitting and neglected all the modes that are far detuned from excitonic transitions as they were deemed to have a negligible effect⁶⁷. However, the correct assessment of the nature of oscillatory 2D signals requires the computation of 2D spectra under the influence of the full spectral density. In order to make such computation feasible, in Supplementary Note 8, we provide an approximate master equation for vibronic dynamics, which takes into account multi-mode mixing effects and quantitatively reproduces numerically exact absorption line shape of the SP. Figure 5d shows the resulting rephasing 2D spectra at waiting time $T = 0$ in the presence of inhomogeneous broadening. The 2D lineshape, shown as a function of excitation and detection wavelengths, is dominated by a diagonal peak excited and detected at 900 nm which coincides with the position of the main absorption peak (see Fig. 5b). To investigate the excited state coherence between vibronic eigenstates $|\psi_{+}\rangle$ and $|\psi_{-}\rangle$, which induce the absorption peaks at 780 and 900 nm, respectively, we focus on a cross-peak R12 marked in Fig. 5d. Figure 5e shows the transient of the cross-peak as a function of the waiting time T where the oscillatory 2D signals originating from electronic ground state manifold, shown in red, are comparable to those of excited state signals, shown in blue. The ground state signals

consist of multiple frequency components below 1600 cm^{-1} , corresponding to the vibrational frequencies ω_k of underdamped intra-pigment modes, as shown in Fig. 5f. It is important to note that the excited state signals include a long-lived oscillatory component with frequency $\sim 1800 \text{ cm}^{-1}$, which is not present in the ground state signals and cannot originate from purely vibrational effects as they exceed the high-frequency cut-off of the environmental spectral density (see Fig. 5a). This component must therefore originate from long-lived vibronic coherence due to multi-mode mixing. The long-lived oscillations at $\Delta' \approx 1800 \text{ cm}^{-1}$ frequency cannot be described by coarse-grained environment models where only a few intra-pigment modes near-resonant with the excitonic splitting $\Delta \approx 1300 \text{ cm}^{-1}$ are weakly damped ($\gamma_k = (1 \text{ ps})^{-1}$), while all the other intra-pigment modes are strongly damped ($\gamma_k = (50 \text{ fs})^{-1}$) or neglected ($s_k = 0$) in 2D simulations (see Supplementary Note 8). Our results demonstrate that while some oscillatory components in 2D spectra can originate from purely vibrational motions, long-lived 2D oscillations can also be the result of a strong vibronic mixing of excitons with a large number of underdamped intra-pigment modes.

Discussion

Employing numerically exact methods and an analytical theory, we have investigated exciton-vibrational dynamics under the complete vibrational spectrum that has been estimated in earlier experiments. We considered two paradigmatic regimes. The first regime, represented by an excitonic dimer in WSCP, is characterized by an excitonic splitting that is smaller than vibrational frequencies of intra-pigment modes. In this case, one main effect of vibronic coupling to the intra-pigment modes is a reduction of the dipole strength of 0-0 transitions of monomers and of their effective coupling strength V_{00} that determines the splitting between absorption peaks in the low-energy spectrum. A second important effect concerns the modulation of the vibrational sideband of optical transitions by a vibronic mixing between 0-0 and 0-1 transitions. Although the vibronic mixing is not strong enough to modulate the low-energy part of absorption spectra of WSCP, it can induce a notable dipole strength redistribution between 0-0 and 0-1 transitions, which cannot be described by approximate theories where the vibronic mixing is ignored.

In the second regime, represented by the SP of the photosynthetic reaction center of purple bacteria, the excitonic splitting is located in the middle of the high frequency part of the intra-pigment vibrational spectrum. In this case, the splitting between main absorption peaks can be even larger than the bare excitonic splitting, due to multi-mode vibronic mixing effects. This regime is found to be particularly suitable for the discovery of new long-lived quantum coherences in photosynthesis. We found that the coherence time of excitonic dynamics is not simply governed by the lifetime of quasi-resonant intra-pigment modes. Rather it is determined by the lifetimes of individual intra-pigment modes involved in a multi-mode vibronic mixing. This implies that approximate theoretical models based on coarse-graining of the high frequency part of the vibrational environments²¹ may underestimate the lifetime of excitonic coherences and could be inappropriate to analyze quantum coherences observed in nonlinear experiments on photosynthetic systems. In addition, our results demonstrate that even if the frequency Δ' of oscillatory 2D signals is not well matched to one of the vibrational frequencies ω_k of intra-pigment modes, the long-lived 2D oscillations can be vibronic in origin, rather than being purely electronic, as is the case of the SP where $\omega_k \lesssim 1600 \text{ cm}^{-1} < \Delta' \approx 1800 \text{ cm}^{-1}$. This implies that the origin of long-lived oscillatory 2D signals cannot be identified based only on a comparison of the frequency spectrum of nonlinear signals with the vibrational frequency spectrum of underdamped modes. Hence,

we contend that previously ignored multi-mode vibronic effects must be included in the interpretation of nonlinear spectroscopic signals before the current debate regarding the presence and nature of long-lived quantum coherences in pigment-protein complexes can be settled conclusively.

Our results suggest the possibility that the energy transfer dynamics between electronic states, such as excitons and charge-transfer states, could be governed by the multi-mode nature of the total vibrational environments, rather than a few vibrational modes quasi-resonant with electronic energy-gaps (see Supplementary Note 9). The generality of the methods employed here also suggests that our results have a broad scope and can be of relevance in a wide variety of scenarios involving strong hybridization of electronic and vibrational degrees of freedom, such as recent observations of nonadiabatic dynamics in cavity polaritonics^{68,69}. We expect that renormalization effects considered here may open an entirely new toolbox for vibrational reservoir engineering with possible applications in information technologies and polaritonic chemistry.

Data availability

The simulated absorption and 2DES data generated in this study are provided in the Source Data file. The data used in this paper are also available from the authors upon request. Source data are provided with this paper.

Code availability

The codes used in this work are available from the authors upon reasonable request.

Received: 12 January 2022; Accepted: 4 May 2022;

Published online: 25 May 2022

References

- Blankenship, R. E. *Molecular Mechanisms of Photosynthesis* (Wiley-Blackwell, 2002).
- Monshouwer, R., Abrahamsson, M., van Mourik, F. & van Grondelle, R. Superradiance and exciton delocalization in bacterial photosynthetic light-harvesting systems. *J. Phys. Chem. B* **101**, 7241 (1997).
- Trinkunas, G., Herek, J. L., Polívka, T., Sundström, V. & Pullerits, T. Exciton delocalization probed by excitation annihilation in the light-harvesting antenna LH2. *Phys. Rev. Lett.* **86**, 4167 (2001).
- Jordanides, X. J., Scholes, G. D. & Fleming, G. R. The mechanism of energy transfer in the bacterial photosynthetic reaction center. *J. Phys. Chem. B* **105**, 1652 (2001).
- Hu, X., Ritz, T., Damjanović, A., Autenrieth, F. & Schulten, K. Photosynthetic apparatus of purple bacteria. *Q. Rev. Biophys.* **35**, 1 (2002).
- Renger, T. Theory of optical spectra involving charge transfer states: Dynamic localization predicts a temperature dependent optical band shift. *Phys. Rev. Lett.* **93**, 188101 (2004).
- Raszewski, G., Saenger, W. & Renger, T. Theory of optical spectra of photosystem II reaction centers: Location of the triplet state and the identity of the primary electron donor. *Biophys. J.* **88**, 986 (2005).
- van Grondelle, R. & Novoderezhkin, V. I. Energy transfer in photosynthesis: Experimental insights and quantitative models. *Phys. Chem. Chem. Phys.* **8**, 793 (2006).
- Renger, T. Theory of excitation energy transfer: From structure to function. *Photosynth. Res.* **102**, 471 (2009).
- Jumper, C. C., van Stokkum, I. H. M., Mirkovic, T. & Scholes, G. D. Vibronic wavepackets and energy transfer in cryptophyte light-harvesting complexes. *J. Phys. Chem. B* **122**, 6328 (2018).
- Rätsep, M., Linnanto, J. & Freiberg, A. Mirror symmetry and vibrational structure in optical spectra of chlorophyll a. *J. Chem. Phys.* **130**, 194501 (2009).
- Rätsep, M., Cai, Z.-L., Reimers, J. R. & Freiberg, A. Demonstration and interpretation of significant asymmetry in the low-resolution and high-resolution Q_y fluorescence and absorption spectra of bacteriochlorophyll a. *J. Chem. Phys.* **134**, 024506 (2011).
- Pieper, J. et al. Excitonic energy level structure and pigment-protein interactions in the recombinant water-soluble chlorophyll protein. I. Difference fluorescence line-narrowing. *J. Phys. Chem. B* **115**, 4042 (2011).
- Pieper, J., Artene, P., Rätsep, M., Pajusalu, M. & Freiberg, A. Evaluation of electron-phonon coupling and spectral densities of pigment-protein complexes by line-narrowed optical spectroscopy. *J. Phys. Chem. B* **122**, 9289 (2018).
- Zazubovich, V., Tibe, I. & Small, G. J. Bacteriochlorophyll a Franck-Condon factors for the $S_0 \rightarrow S_1(Q_y)$ transition. *J. Phys. Chem. B* **105**, 12410 (2001).
- Policht, V. R., Niedringhaus, A. & Ogilvie, J. P. Characterization of vibrational coherence in monomeric bacteriochlorophyll a by two-dimensional electronic spectroscopy. *J. Phys. Chem. Lett.* **9**, 6631 (2018).
- Bukartė, E., Haufe, A., Paleček, D., Büchel, C. & Zigmantas, D. Revealing vibronic coupling in chlorophyll c1 by polarization-controlled 2D electronic spectroscopy. *Chem. Phys.* **530**, 110643 (2020).
- Irgen-Giorgio, S., Spencer, A. P., Hutson, W. O. & Harel, E. Coherences of bacteriochlorophyll a uncovered using 3D-electronic spectroscopy. *J. Phys. Chem. Lett.* **9**, 6077 (2018).
- Meneghin, E., Pedron, D. & Collini, E. Characterization of the coherent dynamics of bacteriochlorophyll a in solution. *Chem. Phys.* **519**, 85 (2019).
- Rivera, E., Montemayor, D., Masia, M. & Coker, D. F. Influence of site-dependent pigment-protein interactions on excitation energy transfer in photosynthetic light harvesting. *J. Phys. Chem. B* **117**, 5510 (2013).
- Blau, S. M. et al. Local protein solvation drives direct down-conversion in phycobiliprotein PC645 via incoherent vibronic transport. *Proc. Natl Acad. Sci. USA* **115**, E3342 (2018).
- Prior, J., Chin, A. W., Huelga, S. F. & Plenio, M. B. Efficient simulation of strong system-environment interactions. *Phys. Rev. Lett.* **105**, 050404 (2010).
- Chin, A. W., Datta, A., Caruso, F., Huelga, S. F. & Plenio, M. B. Noise-assisted energy transfer in quantum networks and light-harvesting complexes. *N. J. Phys.* **12**, 065002 (2010).
- Womick, J. M. & Moran, A. M. Vibronic enhancement of exciton sizes and energy transport in photosynthetic complexes. *J. Phys. Chem. B* **115**, 1347 (2011).
- Chin, A. W. et al. The role of non-equilibrium vibrational structures in electronic coherence and recoherence in pigment-protein complexes. *Nat. Phys.* **9**, 113 (2013).
- Irish, E. K., Gómez-Bombarelli, R. & Lovett, B. W. Vibration-assisted resonance in photosynthetic excitation-energy transfer. *Phys. Rev. A* **90**, 012510 (2014).
- Dijkstra, A. G., Wang, C., Cao, J. & Fleming, G. R. Coherent exciton dynamics in the presence of underdamped vibrations. *J. Phys. Chem. Lett.* **6**, 627 (2015).
- Novelli, F. et al. Vibronic resonances facilitate excited-state coherence in light-harvesting proteins at room temperature. *J. Phys. Chem. Lett.* **6**, 4573 (2015).
- Iles-Smith, J., Dijkstra, A. G., Lambert, N. & Nazir, A. Energy transfer in structured and unstructured environments: Master equations beyond the Born-Markov approximations. *J. Chem. Phys.* **144**, 044110 (2016).
- Malý, P., Somsen, O. J. G., Novoderezhkin, V. I., Mančal, T. & van Grondelle, R. The role of resonant vibrations in electronic energy transfer. *ChemPhysChem* **17**, 1356 (2016).
- Caycedo-Soler, F. et al. Theory of excitonic delocalization for robust vibronic dynamics in LH2. *J. Phys. Chem. Lett.* **9**, 3446 (2018).
- Engel, G. S. et al. Evidence for wavelike energy transfer through quantum coherence in photosynthetic systems. *Nature* **446**, 782 (2007).
- Lee, H., Cheng, Y.-C. & Fleming, G. R. Coherence dynamics in photosynthesis: Protein protection of excitonic coherence. *Science* **316**, 1462 (2007).
- Panitchayangkoon, G. et al. Long-lived quantum coherence in photosynthetic complexes at physiological temperature. *Proc. Natl Acad. Sci. USA* **107**, 12766 (2010).
- Hildner, R., Brinks, D., Nieder, J. B., Cogdell, R. J. & van Hulst, N. F. Quantum coherent energy transfer over varying pathways in single light-harvesting complexes. *Science* **340**, 1448 (2013).
- Romero, E. et al. Quantum coherence in photosynthesis for efficient solar-energy conversion. *Nat. Phys.* **10**, 676 (2014).
- Fuller, F. D. et al. Vibronic coherence in oxygenic photosynthesis. *Nat. Chem.* **6**, 706 (2014).
- Christensson, N., Kauffmann, H. F., Pullerits, T. & Mančal, T. Origin of long-lived coherences in light-harvesting complexes. *J. Phys. Chem. B* **116**, 7449 (2012).
- Butkus, V., Valkunas, L. & Abramavicius, D. Molecular vibrations-induced quantum beats in two-dimensional electronic spectroscopy. *J. Chem. Phys.* **137**, 044513 (2012).
- Plenio, M. B., Almeida, J. & Huelga, S. F. Origin of long-lived oscillations in 2D-spectra of a quantum vibronic model: Electronic versus vibrational coherence. *J. Chem. Phys.* **139**, 235102 (2013).

41. Tiwari, V., Peters, W. K. & Jonas, D. M. Electronic resonance with anticorrelated pigment vibrations drives photosynthetic energy transfer outside the adiabatic framework. *Proc. Natl Acad. Sci. USA* **110**, 1203 (2013).
42. Chenu, A., Christensson, N., Kauffmann, H. F. & Mančal, T. Enhancement of vibronic and ground-state vibrational coherences in 2D spectra of photosynthetic complexes. *Sci. Rep.* **3**, 2029 (2013).
43. Huelga, S. F. & Plenio, M. B. Vibrations, quanta and biology. *Contemp. Phys.* **54**, 181 (2013).
44. Duan, H. G. et al. Nature does not rely on long-lived electronic quantum coherence for photosynthetic energy transfer. *Proc. Natl Acad. Sci. USA* **114**, 8493 (2017).
45. Thyryhaug, E. et al. Identification and characterization of diverse coherences in the Fenna–Matthews–Olson complex. *Nat. Chem.* **10**, 780 (2018).
46. Lim, J. et al. Multicolor quantum control for suppressing ground state coherences in two-dimensional electronic spectroscopy. *Phys. Rev. Lett.* **123**, 233201 (2019).
47. Cao, J. et al. Quantum biology revisited. *Sci. Adv.* **6**, eaaz4888 (2020).
48. Novoderezhkin, V. I., Palacios, M. A., van Amerongen, H. & van Grondelle, R. Energy-transfer dynamics in the LHClI complex of higher plants: Modified redfield approach. *J. Phys. Chem. B* **108**, 10363 (2004).
49. Abramavicius, D. & Mukamel, S. Energy-transfer and charge-separation pathways in the reaction center of photosystem II revealed by coherent two-dimensional optical spectroscopy. *J. Chem. Phys.* **133**, 184501 (2010).
50. Lewis, K. L. M. et al. Simulations of the two-dimensional electronic spectroscopy of the photosystem II reaction center. *J. Phys. Chem. A* **117**, 34 (2013).
51. Khmel'nitskiy, A., Reinot, T. & Jankowiak, R. Mixed upper exciton state of the special pair in bacterial reaction centers. *J. Phys. Chem. B* **123**, 852 (2019).
52. Chin, A. W., Rivas, A., Huelga, S. F. & Plenio, M. B. Exact mapping between system-reservoir quantum models and semi-infinite discrete chains using orthogonal polynomials. *J. Math. Phys.* **51**, 092109 (2010).
53. Tamascelli, D., Smirne, A., Huelga, S. F. & Plenio, M. B. Nonperturbative treatment of non-Markovian dynamics of open quantum systems. *Phys. Rev. Lett.* **120**, 030402 (2018).
54. Tamascelli, D., Smirne, A., Lim, J., Huelga, S. F. & Plenio, M. B. Efficient simulation of finite-temperature open quantum systems. *Phys. Rev. Lett.* **123**, 090402 (2019).
55. Tanimura, Y. & Kubo, R. Time evolution of a quantum system in contact with a nearly Gaussian–Markoffian noise bath. *J. Phys. Soc. Jpn.* **58**, 101 (1989).
56. Warshel, A. & Parson, W. W. Spectroscopic properties of photosynthetic reaction centers. 1. Theory. *J. Am. Chem. Soc.* **109**, 6143 (1987).
57. Madjet, M. E.-A., Müh, F. & Renger, T. Deciphering the influence of short-range electronic couplings on optical properties of molecular dimers: Application to “special pairs” in photosynthesis. *J. Phys. Chem. B* **113**, 12603 (2009).
58. Kell, A., Feng, X., Reppert, M. & Jankowiak, R. On the shape of the phonon spectral density in photosynthetic complexes. *J. Phys. Chem. B* **117**, 7317 (2013).
59. Renger, T. & Marcus, R. A. On the relation of protein dynamics and exciton relaxation in pigment-protein complexes: An estimation of the spectral density and a theory for the calculation of optical spectra. *J. Chem. Phys.* **116**, 9997 (2002).
60. Dinh, T.-C. & Renger, T. Towards an exact theory of linear absorbance and circular dichroism of pigment-protein complexes: Importance of non-secular contributions. *J. Chem. Phys.* **142**, 034104 (2015).
61. Reppert, M., Kell, A., Pruitt, T. & Jankowiak, R. Comments on the optical lineshape function: Application to transient hole-burned spectra of bacterial reaction centers. *J. Chem. Phys.* **142**, 094111 (2015).
62. Kreisbeck, C. & Kramer, T. Long-lived electronic coherence in dissipative exciton dynamics of light-harvesting complexes. *J. Phys. Chem. Lett.* **3**, 2828 (2012).
63. Madjet, M. E., Abdurahman, A. & Renger, T. Intermolecular Coulomb couplings from ab initio electrostatic potentials: Application to optical transitions of strongly coupled pigments in photosynthetic antennae and reaction centers. *J. Phys. Chem. B* **110**, 17268 (2006).
64. Brixner, T., Mančal, T., Stiopkin, I. V. & Fleming, G. R. Phase-stabilized two-dimensional electronic spectroscopy. *J. Chem. Phys.* **121**, 4221 (2004).
65. Jonas, D. M. Two-dimensional femtosecond spectroscopy. *Annu. Rev. Phys. Chem.* **54**, 425 (2003).
66. Mukamel, S. *Principles of Nonlinear Optical Spectroscopy* (Oxford University Press, 1995).
67. Nalbach, P., Braun, D. & Thorwart, M. Exciton transfer dynamics and quantumness of energy transfer in the Fenna–Matthews–Olson complex. *Phys. Rev. E* **84**, 041926 (2011).
68. Vergauwe, R. M. A. et al. Modification of enzyme activity by vibrational strong coupling of water. *Angew. Chem. Int. Ed.* **58**, 15324 (2019).
69. Lather, J., Bhatt, P., Thomas, A., Ebbesen, T. W. & George, J. Cavity catalysis by cooperative vibrational strong coupling of reactant and solvent molecules. *Angew. Chem. Int. Ed.* **58**, 10635 (2019).
70. Adolphs, J. & Renger, T. How proteins trigger excitation energy transfer in the FMO complex of green sulfur bacteria. *Biophys. J.* **91**, 2778 (2006).

Acknowledgements

F.C.-S., A.M., J.L., S.F.H., and M.B.P. acknowledge financial support by the ERC Synergy grants BioQ and HyperQ, and support by the state of Baden-Württemberg through bwHPC and the German Research Foundation (DFG) through grant no INST 40/575-1 FUGG (JUSTUS 2 cluster). A.M. acknowledges financial support by an IQST PhD fellowship. T.R. acknowledges financial support by the Austrian Science Fund (FWF): P 33155-NBL.

Author contributions

F.C.-S., T.R., S.F.H., and M.B.P. initiated this work. F.C.-S., A.M., and J.L. performed numerical simulations. All authors discussed the results and contributed to the writing of the paper.

Funding

Open Access funding enabled and organized by Projekt DEAL.

Competing interests

The authors declare no competing interests.

Additional information


Supplementary information The online version contains supplementary material available at <https://doi.org/10.1038/s41467-022-30565-4>.

Correspondence and requests for materials should be addressed to S. F. Huelga or M. B. Plenio.

Peer review information *Nature Communications* thanks the anonymous reviewers for their contribution to the peer review of this work. Peer reviewer reports are available.

Reprints and permission information is available at <http://www.nature.com/reprints>

Publisher's note Springer Nature remains neutral with regard to jurisdictional claims in published maps and institutional affiliations.

 **Open Access** This article is licensed under a Creative Commons Attribution 4.0 International License, which permits use, sharing, adaptation, distribution and reproduction in any medium or format, as long as you give appropriate credit to the original author(s) and the source, provide a link to the Creative Commons license, and indicate if changes were made. The images or other third party material in this article are included in the article's Creative Commons license, unless indicated otherwise in a credit line to the material. If material is not included in the article's Creative Commons license and your intended use is not permitted by statutory regulation or exceeds the permitted use, you will need to obtain permission directly from the copyright holder. To view a copy of this license, visit <http://creativecommons.org/licenses/by/4.0/>.

© The Author(s) 2022